

Framed link presentations of 3-manifolds by an $O(n^2)$ algorithm, II: colored complexes and their wings *

Sóstenes Lins and Ricardo Machado

June 7, 2022

Abstract

This is part 2 of a 3-part article where we provide an $O(n^2)$ -algorithm to produce a surgery presentation of a 3-manifold induced by a gem with a resolution. In this part we produce a sequence of colored simplicial 2-complexes which are inverses and dual to the sequence of gems produced in the first part. Two enriching novelties that the dual situation yields are the rank of the DPL-faces which keep appearing and the possibility of defining *wings* for these complexes. These notions are really the essence which inhibits exponentiability. The first because the refinements of the DPL-faces that keep appearing are idempotent: the second refinement of a DPL-face is isomorphic to its first refinement. The wings, via a weight enhanced Tutte's barycentric embedding of a planar map, produce the unexpected reformulation of a 3-dimensional problem into a 2-dimensional one. The number of 1-simplices in a wing of the initial complex in the sequence is $4n - 1$ and at each one of the $(n - 1)$ steps we sum 4 new edges. The total number of edges in each one of the pair of final wings is bounded by $8n - 5$. Tutte's method is applied $O(n)$ times to each one of the wings in the final pair. The final pair of wings is the only place where we need coordinates. These planar coordinates are transferred to 3D-ones by a simple pair of rotations of the wings.

1 The sequence of combinatorial 2-complexes: $\mathcal{H}_1^*, \mathcal{H}_2^*, \dots, \mathcal{H}_{2n}^*$

The inverse of a 2-dipole thickening is a *3-dipole slimming*. We need to consider the combinatorial duals of some objects. To a 2-dipole corresponds a *pillow* in the dual, namely two tetrahedra with two faces in common. To a 3-dipole (or blob) and a color involved in it corresponds a *balloon* in the dual. The balloon is formed by two tetrahedra with 3 faces in common together with a triangle sharing an edge with the two tetrahedra. The dual of a 3-dipole slimming is a *balloon-pillow move*, or *bp-move*. A sequence of these moves related to the r_5^{24} -example are depicted in Figs. 17 to 22.

There is an important topological interpretation between primal and dual complexes, given in the book [Lin95] pages 38, 39. Let's take a look at this interpretation in our context, which will help us to understand the PL-embedding $E\mathcal{H}_\ell^*$. In what follows the letters Z, U, D and T stands for the dimensions 0, 1, 2 and 3 of the PL-faces.

- i. a vertex v in $G \rightleftharpoons$ a solid PL-tetrahedron or TPL-face, named T_v in the dual of the gem whose ZPL-faces are labelled z_0, z_1, z_2 e z_3^v ; in this work is enough to work with the boundary of a TPL-face, denoted by $\partial\text{TPL-face}$;
- ii. an i colored edge e_i in $G \rightleftharpoons$ a set of i -colored 2-simplices defining a DPL_i -face in the dual of the gem whose ZPL-faces are labelled with the 3 colors distinct from i ;
- iii. a bigon B_{ij} using the colors i, j in $G \rightleftharpoons$ a set of 1-simplices b_{ij} in $E\mathcal{H}_\ell^*$ defining a UPL_{ij} -face whose ends are labelled h, k , where (h, i, j, k) is a permutation of $(0, 1, 2, 3)$;
- iv. a \widehat{i} -residue V_i in $G \rightleftharpoons$ a 0-simplex in $E\mathcal{H}_\ell^*$ defining a ZPL_i -face.

*2010 Mathematics Subject Classification: 57M25 and 57Q15 (primary), 57M27 and 57M15 (secondary)

We are going to define the combinatorial PL 2-dimensional complex \mathcal{H}_1^* and so, build $E\mathcal{H}_1^*$. Let $j \in \{1, \dots, 2n\}$, define v_0^j, v_1^j and v_2^j as the vertices of $2n$ equilateral triangles and subdivide as in figure 1 defining v_3^j, v_4^j and v_5^j . The scheme of colors depends of parity, if j is odd, all the triangles are 3-colored, otherwise triangles $v_0^j v_3^j v_1^j$ are 2-colored, defining the DPL_2 -faces, triangles $v_0^j v_4^j v_3^j$ and $v_2^j v_3^j v_4^j$ are 1-colored, defining the DPL_1 -faces, and the triangles $v_1^j v_3^j v_5^j$ and $v_2^j v_5^j v_3^j$ are 0-colored, defining the DPL_0 -faces.

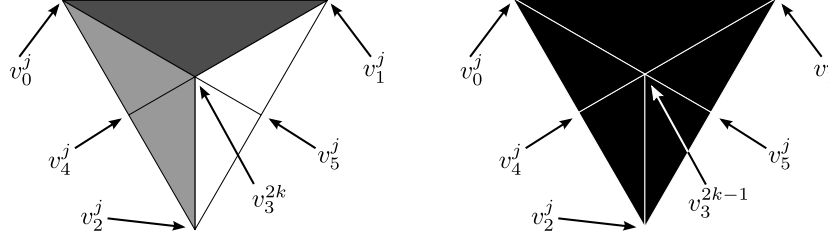


Figure 1: DPL-faces of \mathcal{H}_1^*

We are going to build $E\mathcal{H}_1^*$ using an application from the vertices of \mathcal{H}_1^* to points in \mathbb{R}^3 keeping combinatorial isomorphism if restricted to a j .

Define the image of v_3^j as $z_3^j = (0, 0, 2n - j)$, the image of $v_0^j, v_1^j, v_2^j, v_4^j$ and v_5^j as z_0, z_1, z_2, a_1 and b_1 respectively, such that z_0, z_1, z_2, z_3^1 form a regular tetrahedron, a_1 is the middle point of segment $z_0 z_2$ and b_1 is the middle point of segment $z_1 z_2$.

The dual of a $\hat{3}$ -residue is a ZPL-face named z_3^j where j is even. The dual of the 03-gon is the set of 1-simplices $z_1 z_5$ and $z_5 z_2$, the dual of the 13-gon is the set of 1-simplices $z_0 z_4$ and $z_4 z_2$, the dual of the 23-gon is the 1-simplex $z_0 z_1$, the dual of the 01-gon relative to vertices $u-v$ is the 1-simplex $z_2 z_3^v$, the dual of the 02-gon relative to vertices $u-v$ is the 1-simplex $z_1 z_3^v$, the dual of the 12-gon relative to vertices $u-v$ is the 1-simplex $z_0 z_3^v$. The dual of a 3-colored edge $u'-u$ is the image of DPL_3 -face with odd index u in the vertices, the dual of a i -colored edge $u-v$ with $i \in \{0, 1, 2\}$ is the DPL_i -face with even index v . The dual of vertex u is a tetrahedron made by images of the DPL-faces with index u and $u + 1$.

Before we understand the set \mathcal{H}_ℓ^* , and it's embedding, we are going to understand the dual of the $(pb)^*$ -move and it's inverse. In the primal, to apply a $(pb)^*$ -move, we need a blob and a 0- or 1-colored edge. The dual of this set is the *balloon*. The *balloon's head* is the dual of the blob, and the *balloon's tail* is the dual of the i -edge. To make it easier to understand, the pb -move can be factorable into a 3-dipole move followed by a 2-dipole move, so in dual, it's a smash of the head of the balloon followed by the pillow move described in the book [Lin95], page 39. So, instead of applying two moves, we can perform just one. This is easier to implement and is faster. This is the *balloon-pillow* move. It is described below using a generic 0-colored balloon's tail, of which we just draw the contour. (The specific triangulation is P_{2k-1} , defined in the sequel.)

1. create two 0-simplices $b_{q'}$ and $b_{q''}$ and define the image of v_5^u, v_5^v and $v_5^{v'}$, as $b_{q'}, b_k$ and $b_{k''}$,
2. make two copies of the DPL_0 -face, if necessary, subdivide it, from the middle vertex of the segment $z_2 z_1$ to the other exterior 0-simplex,
3. change the color of the DPL_m -face, $m \in \{1, 2\}$ corresponding to the medial layer of the pillow as in Fig. 2.

Figures 4 and 5 show the effect in the colors of the central level of the balloon when its tail is 0-colored or 1-colored. The choice of the letters P, B, R, G in the set of theorem below comes from the colors $0 = (P)ink$, $1 = (B)lue$, $2 = (R)ed$ and $3 = (G)reen$. In the next proposition R_{2k-1}^b is a DPL_2 -face which is inside the pillow neighboring a DPL_1 -face. Similarly R_{2k-1}^p is a DPL_2 -face which is inside the pillow neighboring a DPL_0 -face.

(1.1) Proposition. *The combinatorial simplicial complex \mathcal{H}_ℓ^* , $1 \leq \ell \leq 2n$, can be embedded in \mathbb{R}^3 where each DPL-faces combinatorially isomorphic to one in the set*

$$\{G, P_{2k-1}, P_{2k-1}', B_{2k-1}, B_{2k-1}', R_{2k-1}^b, R_{2k-1}^p \mid k \in \mathbb{N}\},$$

described in Fig. 3, where the index means the number of edges indicated.

we use arithmetic mod $2n$

u is odd, $u' = u - 1$

$v = u + 1$, $v' = u + 2$

s don't need to be $r + 1$

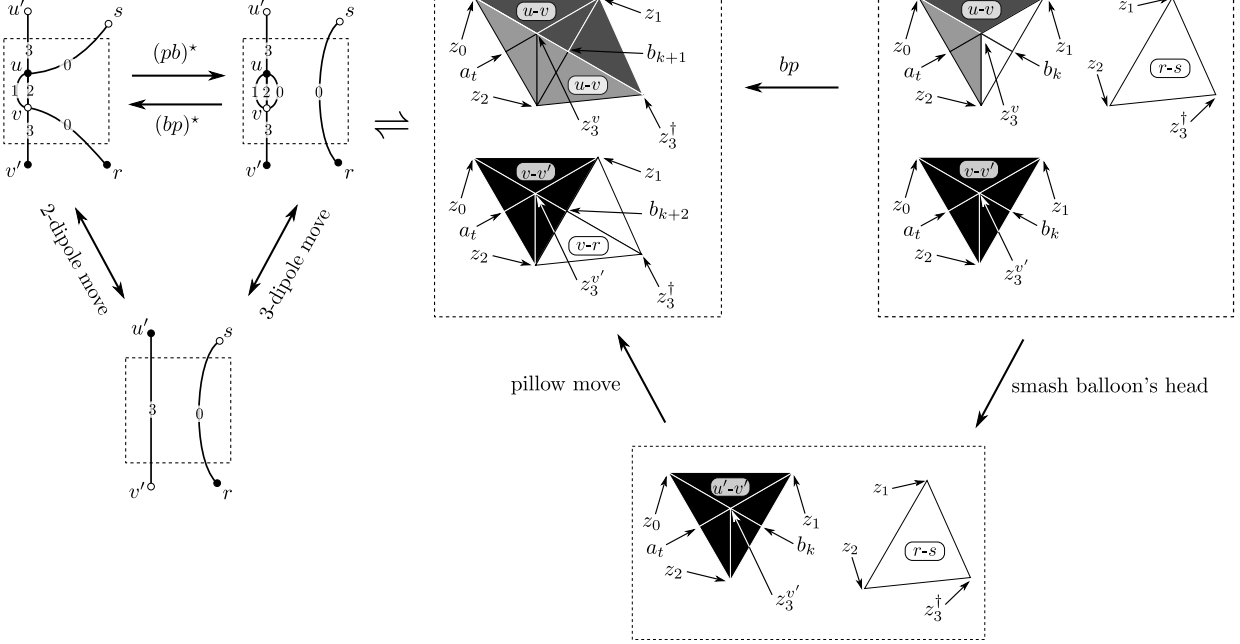


Figure 2: Primal and dual bp -moves

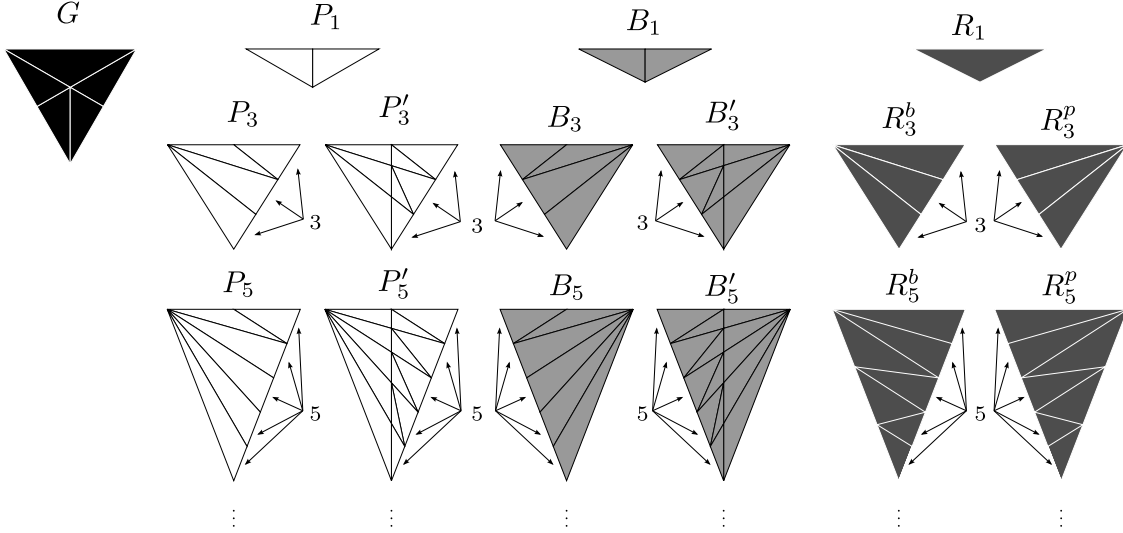


Figure 3: All kinds of DPL-faces

Proof. We need to fix a notation for the head of the balloon, instead of drawing all the DPL-faces of the head, we just draw one DPL₃-face and put a label $u'-v'$. If the balloon's tail, is of type P_1 , by apply bp -move we can see at figure 4 that we get a DPL₁-face of type B_3 and a DPL₂-face of type R_3^b . The others DPL-faces are already known. If the balloon's tail, is of type B_3 , by apply bp -move, we need to refine the tail and the copies, otherwise we can't build a pillow because some 2-simplices would be collapsed, so we get two DPL₁-faces of

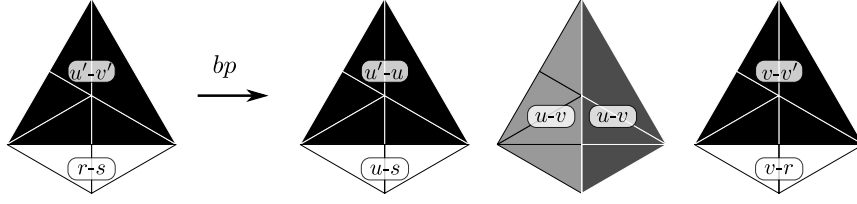


Figure 4: Pillow-balloon move with balloon's tail of type P_1

type B'_3 , one DPL_0 -face of type P_5 and a DPL_2 -face R_5^p . The others DPL -faces are already known.

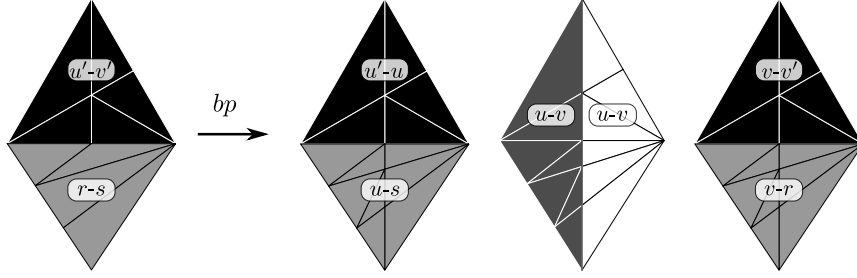


Figure 5: Pillow-balloon move with balloon's tail of type B_3

In what follows given $X \in \{P'_{2k-1}, B'_{2k-1}\}$ denote by \hat{X} the copy of X which is a DPL -face of the PL-tetrahedra whose DPL_3 -face is below the similar DPL_3 -face of the other PL-tetrahedra which completes the pillow in focus. In face of this convention we have that, if balloon's tail is of type

- P_{2k-1} , then by applying a bp -move, we get types $P'_{2k-1}, \hat{P}'_{2k-1}, B_{2k+1}, R_{2k-1}^b$
- P'_{2k-1} , then by applying a bp -move, we get types $P_{2k-1}, B_{2k+1}, R_{2k-1}^b$
- B_{2k-1} , then by applying a bp -move, we get types $B'_{2k-1}, \hat{B}'_{2k-1}, P_{2k+1}, R_{2k-1}^p$
- B'_{2k-1} , then by applying a bp -move, we get types $B_{2k-1}, P_{2k+1}, R_{2k-1}^p$

□

It is worthwhile to mention, in view of the above proof, that each DPL -face is refined at most one time. So, $X'' = X'$, and this idempotency is a crucial property inhibiting the exponentiality of the process.

2 Upper bounds for the number of simplices of the complex \mathcal{H}_{2n}^*

Now we are able to provide quadratic upper bound for the number of i -simplices, $i \in \{0, 1, 2\}$ of \mathcal{H}_ℓ^* .

2.1 Upper bound for the 0-simplices of \mathcal{H}_ℓ^*

In figures 6 and 7, we use a white disk for vertices which its images for the embedding \mathcal{H}_ℓ^* is inalterd from $\mathcal{H}_{\ell-1}^*$ and a black and white disk for the new ones.

(2.1) Theorem. *The quadratic expression $3n^2 - 5n + 9$ is an upper bound for the number of 0-simplices of the 2-complex \mathcal{H}_{2n}^* induced by a resolution of a 3-gem G with $2n$ vertices.*

Proof. We know that \mathcal{H}_1^* has exactly z_0, z_1, z_2, z_4, z_5 and $z_3^j, j \in \{1, \dots, 2n\}$ as 0-simplices, which is $2n + 5$ 0-simplices. In first step balloon's tail has to be P_1 or B_1 , so by apply bp -move, we get two new 0-simplices, which inverse image is a black and white disk in Fig. 6 (first part)

In second step the worse case is when balloon's tail is a P_3 or B_3 , generated by last bp -move, so we add $6 \times 1 + 2 = 8$ to the number of 0-simplices in the upper bound. See Fig. 6 (second part).

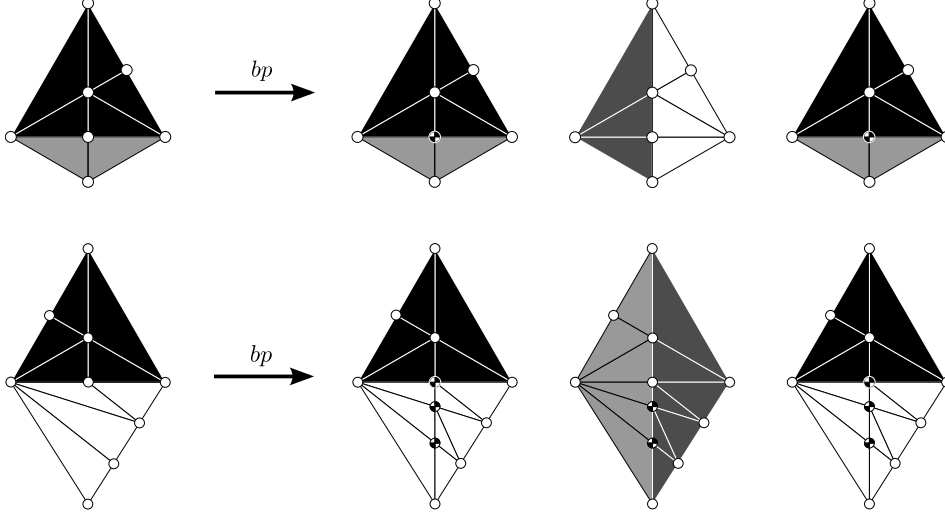


Figure 6: Upper bound for the number of the 0-simplices, first and second steps

In step k we note that worst case is when we use the biggest DPL-face generated by last bp-move, so it means that balloon's tail has to be P_{2k-1} or B_{2k-1} , (in Fig. 7 $j = 2k - 1$) which we add $(6 \cdot (k - 1) + 2)$ 0-simplices.

By adding the number of 0-simplices created by bp-moves from step 1 until step k we get $3k^2 - k$ 0-simplices. As the number of steps is $n - 1$, and we have at the beginning $2n + 5$, we have that $3n^2 - 5n + 9$ is an upper bound for the number of 0-simplices.

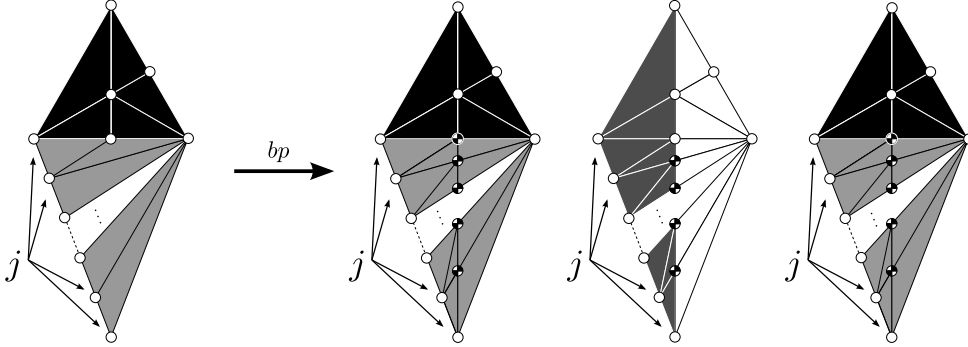


Figure 7: Upper bound for the number of the 0-simplices, j -th step

□

2.2 Upper bound for the 1-simplices of \mathcal{H}_ℓ^*

Now we count the number of 1-simplices, in figures 8 and 9, we emphasize 1-simplices that changes in a bp-move with a dashed line segment.

(2.2) Theorem. *The quadratic expression $11n^2 - 17n + 21$ is an upper bound for the number of 1-simplices of the 2-complex \mathcal{H}_{2n}^* induced by a resolution of a 3-gem G with $2n$ vertices.*

Proof. We know that \mathcal{H}_1^* has exactly $z_0z_1, z_0z_4, z_1z_5, z_2z_5, z_2z_4, z_0z_3^j, z_1z_3^j, z_5z_3^j, z_2z_3^j, z_4z_3^j, j \in \{1, \dots, 2n\}$ as 1-simplices which give us $10n + 5$ 1-simplices. In first step balloon's tail has to be P_1 or B_1 , so by apply bp-move, we add $2 \times 3 = 6$ to the number of 1-simplices in the upper bound.

In second step we know that worst case is when balloon's tail is P_3 or B_3 , see Fig. 8 (second part) and we add $8 + 2 \times 11 - 2 = 28$ to the number of 1-simplices in the upper bound.

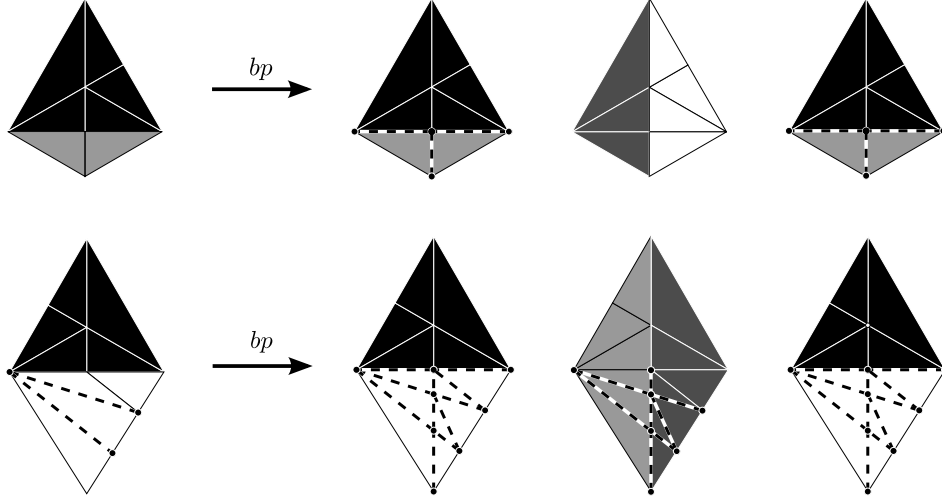


Figure 8: Upper bound for the number of the 1-simplices, first and second steps

In step k , in 0-simplex case, the worst case is when we use the biggest DPL-face generated by last bp-move, so it means that balloon's tail has to be P_{2k-1} or B_{2k-1} , (in Fig. 9, $j = 2k - 1$) and we add $2(3 + 8(k - 1)) + 8(k - 1) - 2(k - 1) = 28k - 22$ to the number of 1-simplices in the upper bound.

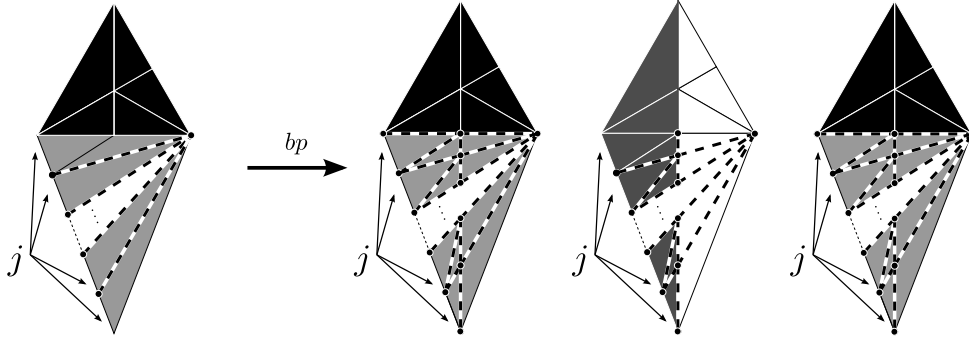


Figure 9: Upper bound for the number of the 1-simplices, j -th step

An upper bound for the number of 1-simplices created by bp-moves in steps $1 \text{---} k$ is $11k^2 - 5k$. As the number of steps is $n - 1$, and we have at the beginning $10n + 5$, it follows that, by adding the arithmetical progression, $11n^2 - 17n + 21$ is an upper bound for the number of 1-simplices. \square

2.3 Upper bound for the 2-simplices of \mathcal{H}_ℓ^\star

Now we count the number of 2-simplices, we detach the 2-simplex set which changes with a delimited region by dashed segment lines

(2.3) Theorem. *The quadratic expression $8n^2 - 20n + 12$ is an upper bound for the number of 2-simplices of the 2-complex \mathcal{H}_{2n}^\star induced by a resolution of a 3-gem G with $2n$ vertices.*

Proof. We know that \mathcal{H}_1^\star has exactly $z_0 z_3^j z_1, z_1 z_3 z_5, z_2 z_5 z_3^j, z_2 z_3^j z_4, z_0 z_4 z_3^j$, $j \in \{1, \dots, 2n\}$ as 2-simplices which give us $10n$ 2-simplices. In first step balloon's tail has to be P_1 or B_1 , so by apply bp-move, we add $2 \cdot 2$ 2-simplices. In second step we add $3 \cdot 8$ and subtract 4

As we know, the worst case in step k is when balloon's tail is P_{2k-1} , or B_{2k-1} . By apply bp-move we add $3 \cdot (8 + 6 \cdot (k - 2))$ and subtract $2 \cdot (k - 1) + 2$, for $k \geq 2$.

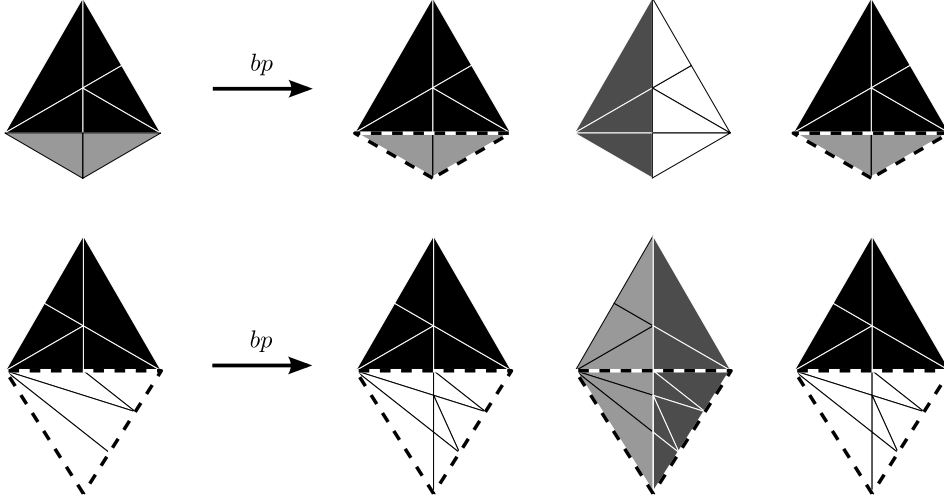


Figure 10: Upper bound for the number of the 2-simplices, first and second steps

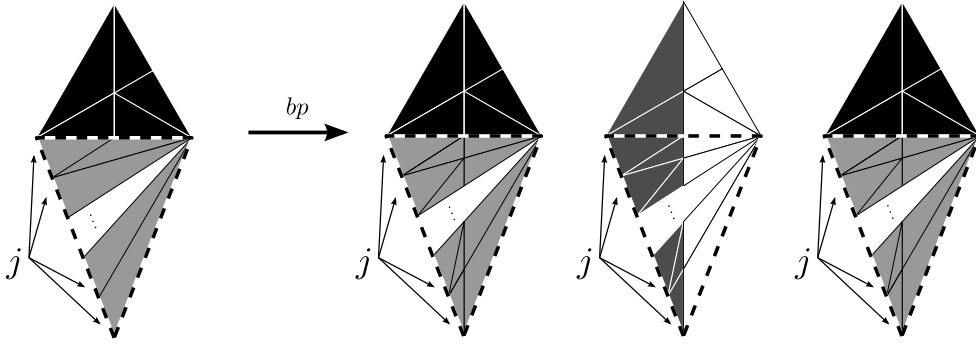


Figure 11: Upper bound for the number of the 2-simplices, j -th step

By adding the number of 2-simplices created by bp-moves from step 1 until step k we get $8k^2 - 4k$ 2-simplices. As the number of steps is $n - 1$, and we have at the beginning $10n$, we have that $8n^2 - 20n + 12$ is an upper bound for the number of 2-simplices. \square

3 Wings

In this section we are going to define another object which is essential to build the embedding $E\mathcal{H}_\ell^*$. The set of all 1-simplices of $E\mathcal{H}_\ell^*$ which are contained in the semi-plane limited by z axis containing a_1 is the *left wing*. The set of all 1-simplices of $E\mathcal{H}_\ell^*$ contained in the semi-plane limited by z axis containing b_1 is the *right wing*. When we say *wings*, we are referring to both the left and the right wings. We denote the wings corresponding to $E\mathcal{H}_\ell^*$ as \mathcal{W}_ℓ .

Restricted to the wings, we call bp-move as *wbp-move* which is explained in figure 12, where balloon's head section is painted with gray, and the part of balloon's tail that is contained in the respective semi plane is the *thick edge*.

Will be useful if we know the wings of all embeddings, so we need a strategy. To apply this move we separate the wings and create some virtual edges, just to make our set to be made of triangles and quadrilaterals. The virtual edges are between z_3^j and z_3^{j+1} 0-simplices, and two a_t or two b_k 0-simplices. To look at the wings as a planar graph, which is better to work, when we make any wbp-move with 1-colored tail we rotate the left wing -30° around the z axis and when we make any wbp-move with 0-colored tail we rotate the right wing 30° around the z axis. Therefore we have both wings in the plane xz . So we get the changes in terms of the graph

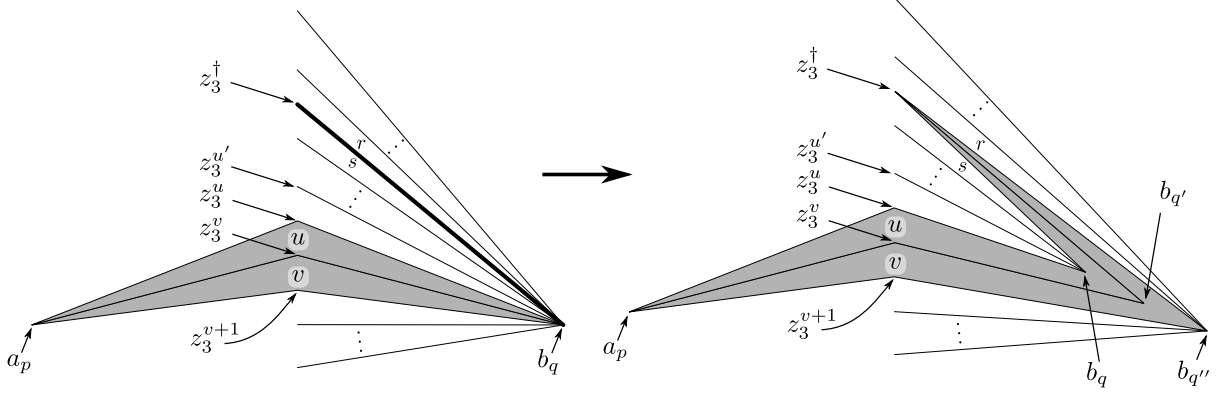


Figure 12: *wbp*-move

of the wings and apply barycentric Tutte's method, [Tut63], [CdVPV03] to get 2D coordinates such that, after correct rotation we get all a_k and b_k in 3D coordinates.

To make the changes from one step to other, we keep counterclockwise vertex rotation. In each step we make the changes of rotations in the vertices of ends of the thick edge.

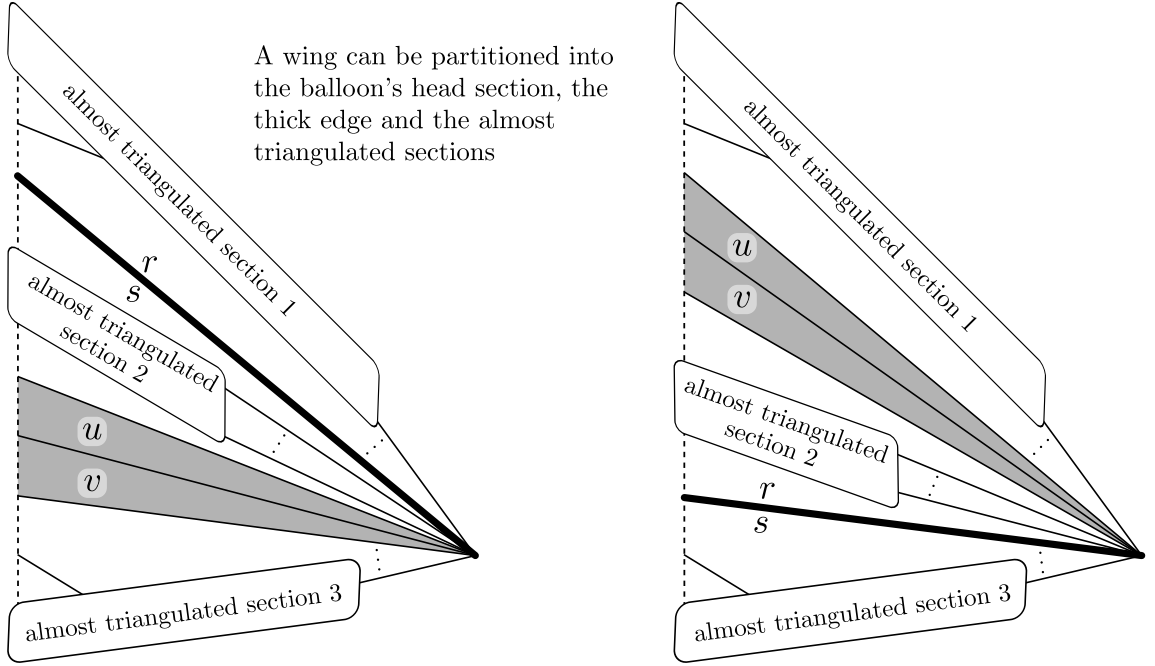
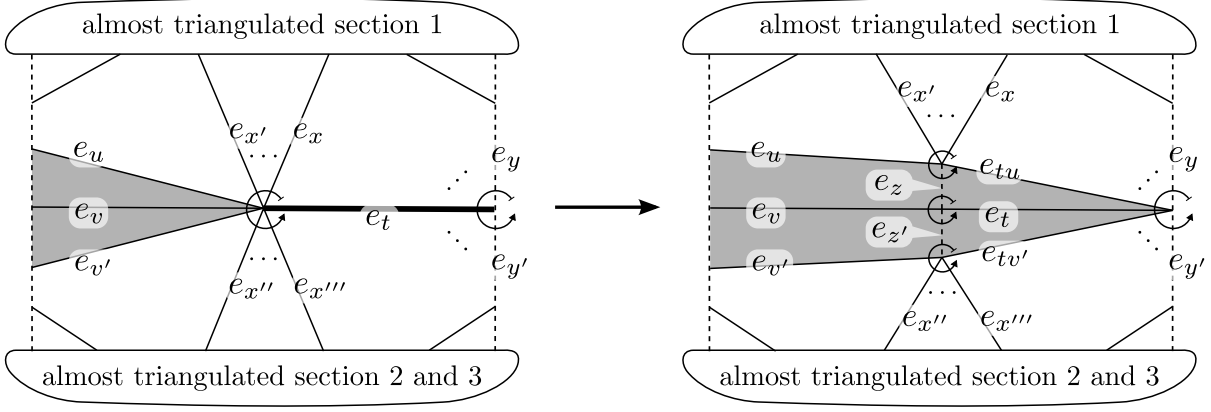


Figure 13: Partitioning a wing, cases thick edge above and thick edge below

The general case is described in Fig. 14 with a scheme that shows explicitly what we need to do. So, we just change the information in terms of rotations, substituting the old rotation information of the two vertices, by the four new rotations.

Before we use Tutte's method we show how to use weights to get a better result. The subgraph of a wing which is a tree and all the edges are the virtual edges connecting two a_k or b_k vertices is the *nervure tree*. We define the weights for the edges of the wings as 1 if the edge is not in the nerv-tree. If the edge is in the nervure tree, to calculate the weight we use the whole wing. Start defining these weights as 0, so from leaves to root, define the weight of an edge as the weight of the vertex incident to it and closer to the leaves minus 1, fig. 15.

For better results, we can apply a linear function $f(x) = ax$, $a > 1$. We can compare in figure 16 the result



$$\begin{aligned}
 (e_x, \dots, e_{x'}, e_u, e_v, e_{v'}, e_{x''}, \dots, e_{x'''}, e_t) &\longrightarrow ((e_x, \dots, e_{x'}, e_u, e_z, e_{tu}), \\
 &\quad (e_z, e_v, e_{z'}, e_t), \\
 &\quad (e_{z'}, e_{v'}, e_{x''}, \dots, e_{x'''}, e_{tv'})) \\
 (e_y, \dots, e_t, \dots, e_{y'}) &\longrightarrow (e_y, \dots, e_{tu}, e_t, e_{tv'}, \dots, e_{y'})
 \end{aligned}$$

Figure 14: Charaterizing a wbp-move by changing the rotation of the planar map corresponding to the wing

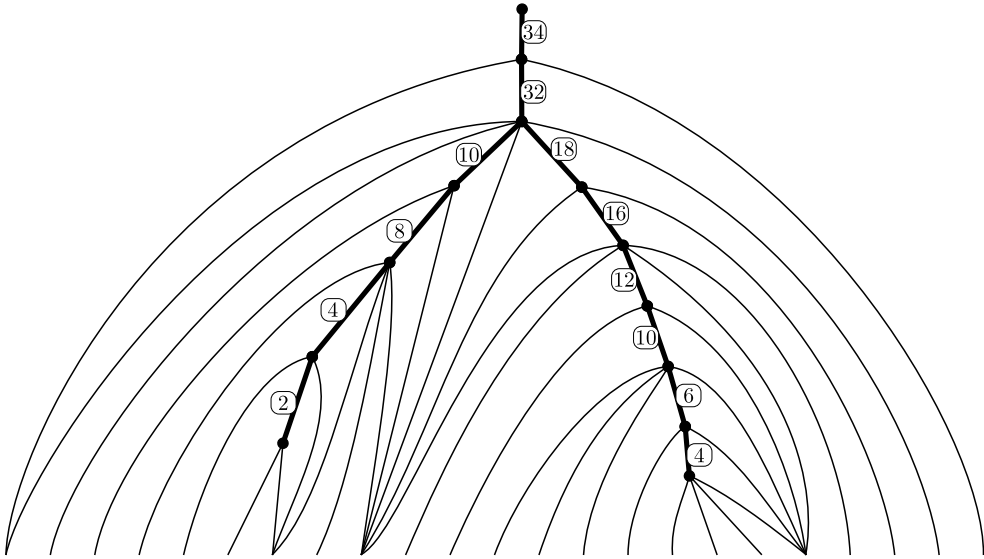


Figure 15: Computing the weights for Tutte's baricentric method via the wing nervure tree

without weight in the left side and using weight with function $f(x) = 3x$ in the right side. In the left side of figure 16, we have one of the 0-simplices with order 10^{-5} distant from z axis, if we work with a bigger graph and use the wings with no weight system we may have some numerical problems when we try to build the embedding $E\mathcal{H}_\ell^*$.

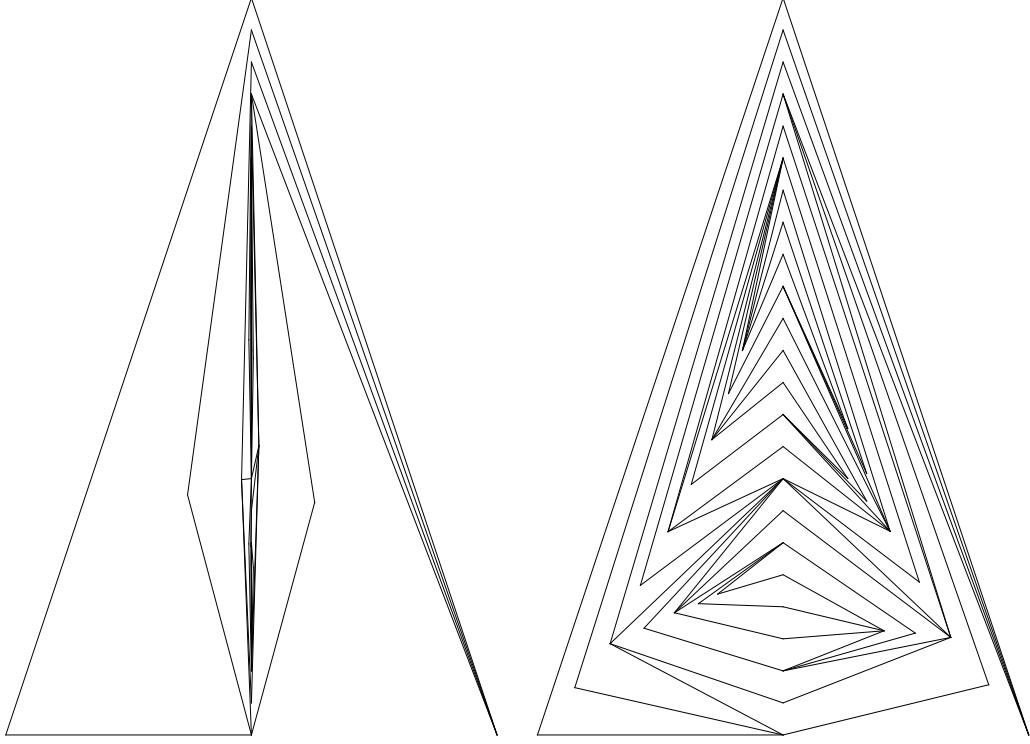


Figure 16: Tutte's embedding without and with the weights (final pair of wings without nervure trees in r_5^{24})

References

- [CdVPV03] É. Colin de Verdière, M. Pocchiola, and G. Vegter. Tutte's barycenter method applied to isotopies. *Computational Geometry*, 26(1):81–97, 2003.
- [Lin95] S. Lins. Gems, Computers, and Attractors for 3-manifolds. *Knots and Everything*, pages 1–450, 1995.
- [Tut63] W.T. Tutte. How to draw a graph. *Proc. London Math. Soc*, 13(3):743–768, 1963.

4 Appendix A:

Wings of the geometric complexes corresponding to r_5^{24}

We present in Figs. 17-21 the passages between left (or right) wings of \mathcal{W}_i and \mathcal{W}_{i+1} corresponding and inducing the geometric complexes \mathcal{H}_i^* 's. In the bottom part of Fig. 22 we present the nervure-free wings of the final complex \mathcal{H}_{12}^* 's. These final pair of wings is the only information needed to proceed and solve 3-dimensional problem of getting the full geometric complex \mathcal{H}_{12}^* , from which the framed link can be easily extracted .

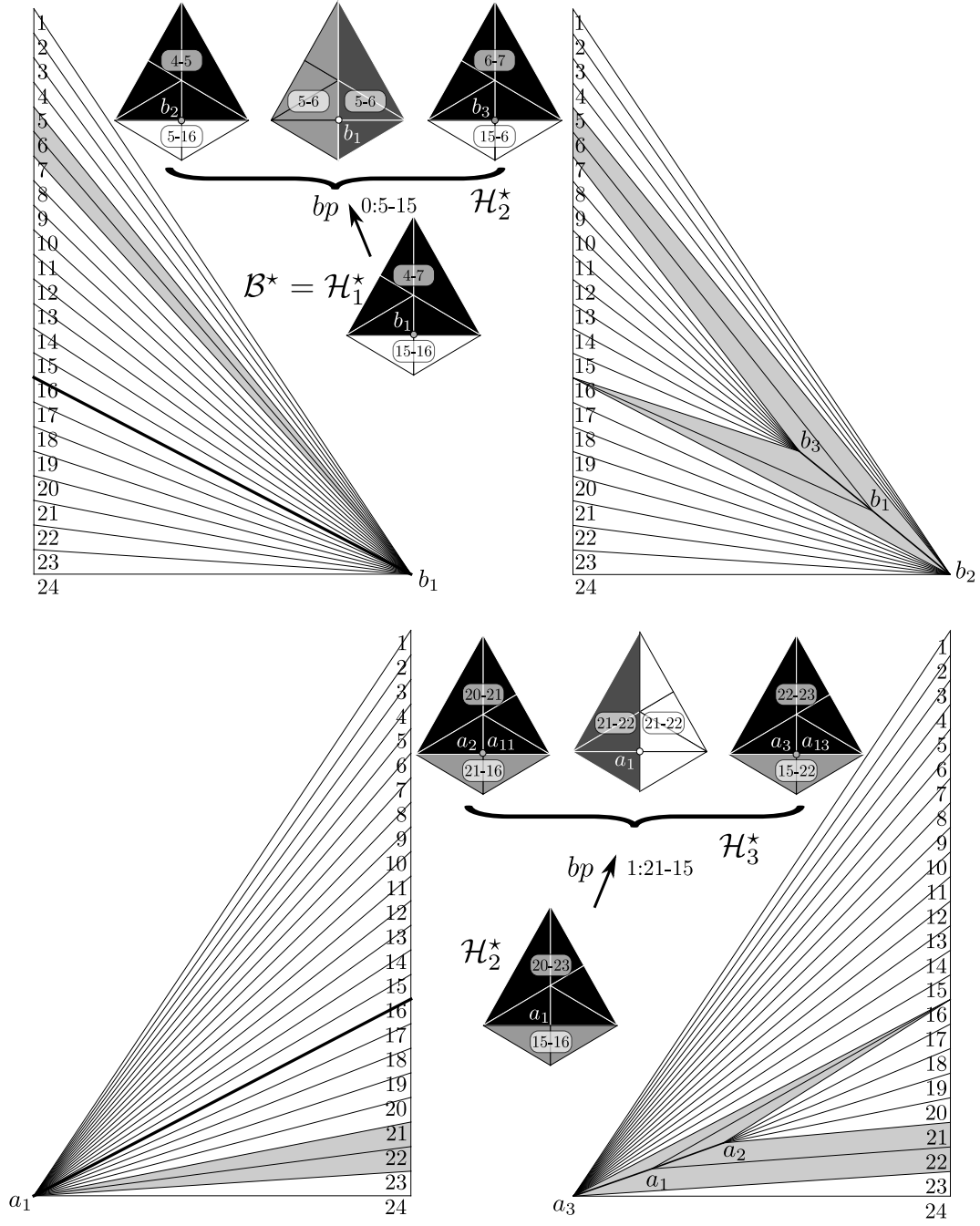


Figure 17: Right wings of complexes \mathcal{H}_1^* , \mathcal{H}_2^* and left wings of complexes \mathcal{H}_2^* , \mathcal{H}_3^* of the r_5^{24} example

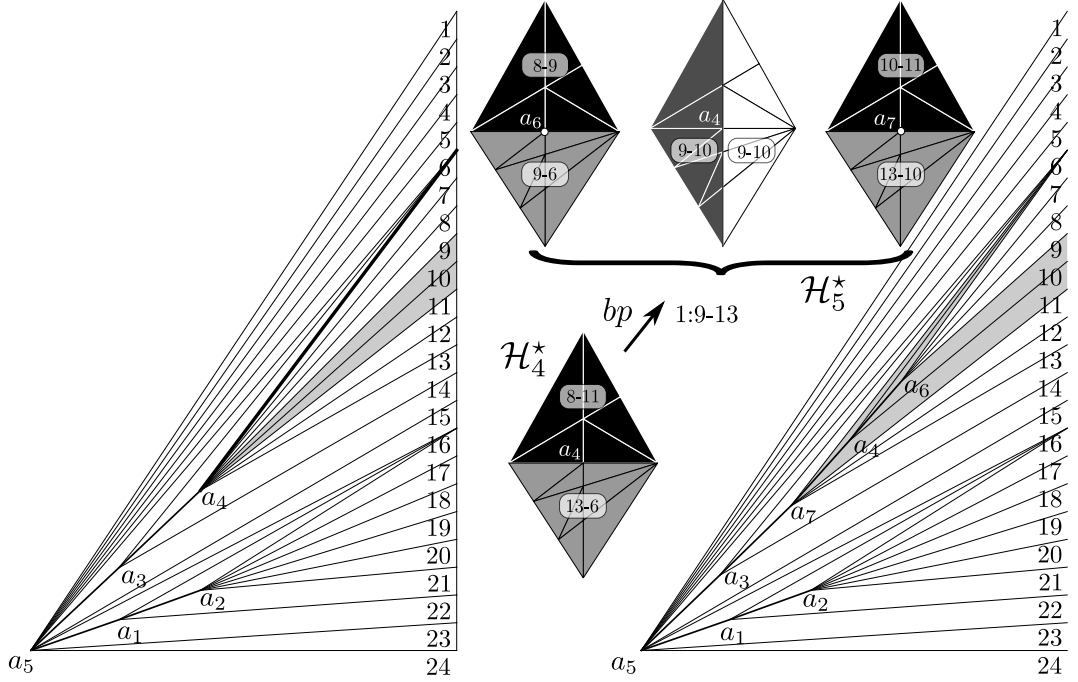
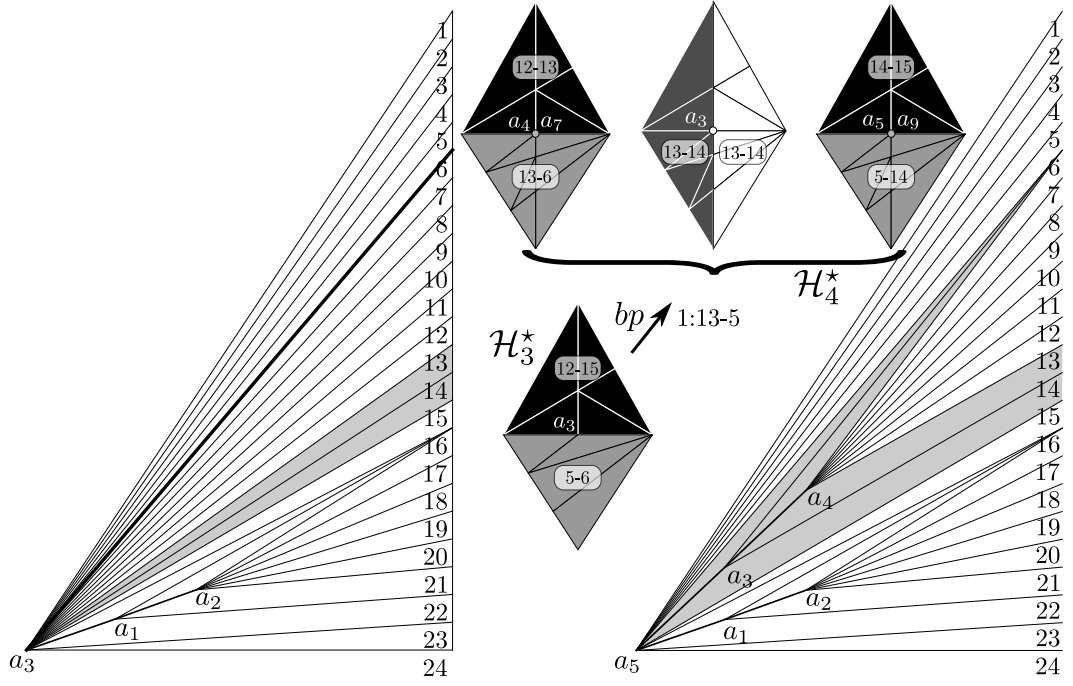


Figure 18: Left wings of complexes \mathcal{H}_3^* , \mathcal{H}_4^* and left wings of complexes \mathcal{H}_4^* , \mathcal{H}_5^* of the r_5^{24} example

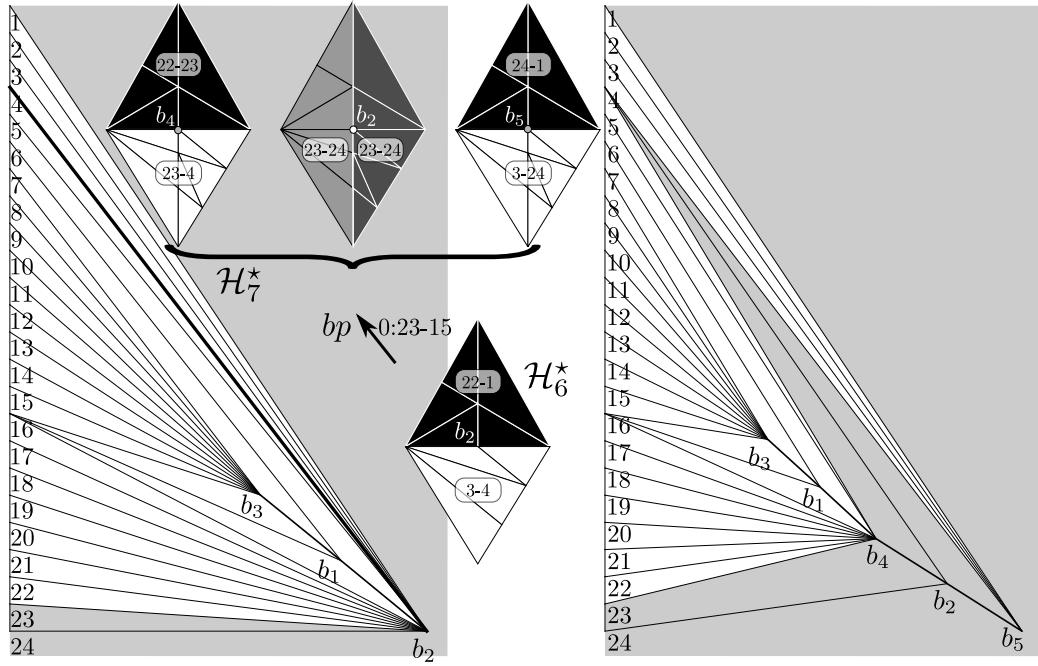
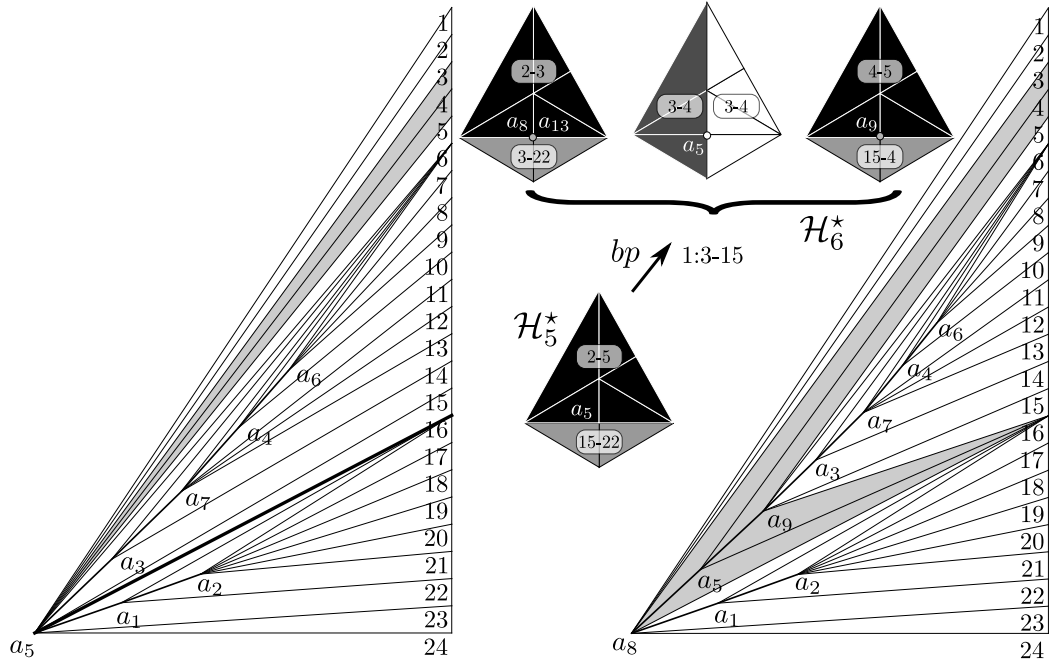


Figure 19: Left wings of complexes \mathcal{H}_5^* , \mathcal{H}_6^* and right wings of complexes \mathcal{H}_6^* , \mathcal{H}_7^* of the r_5^{24} example

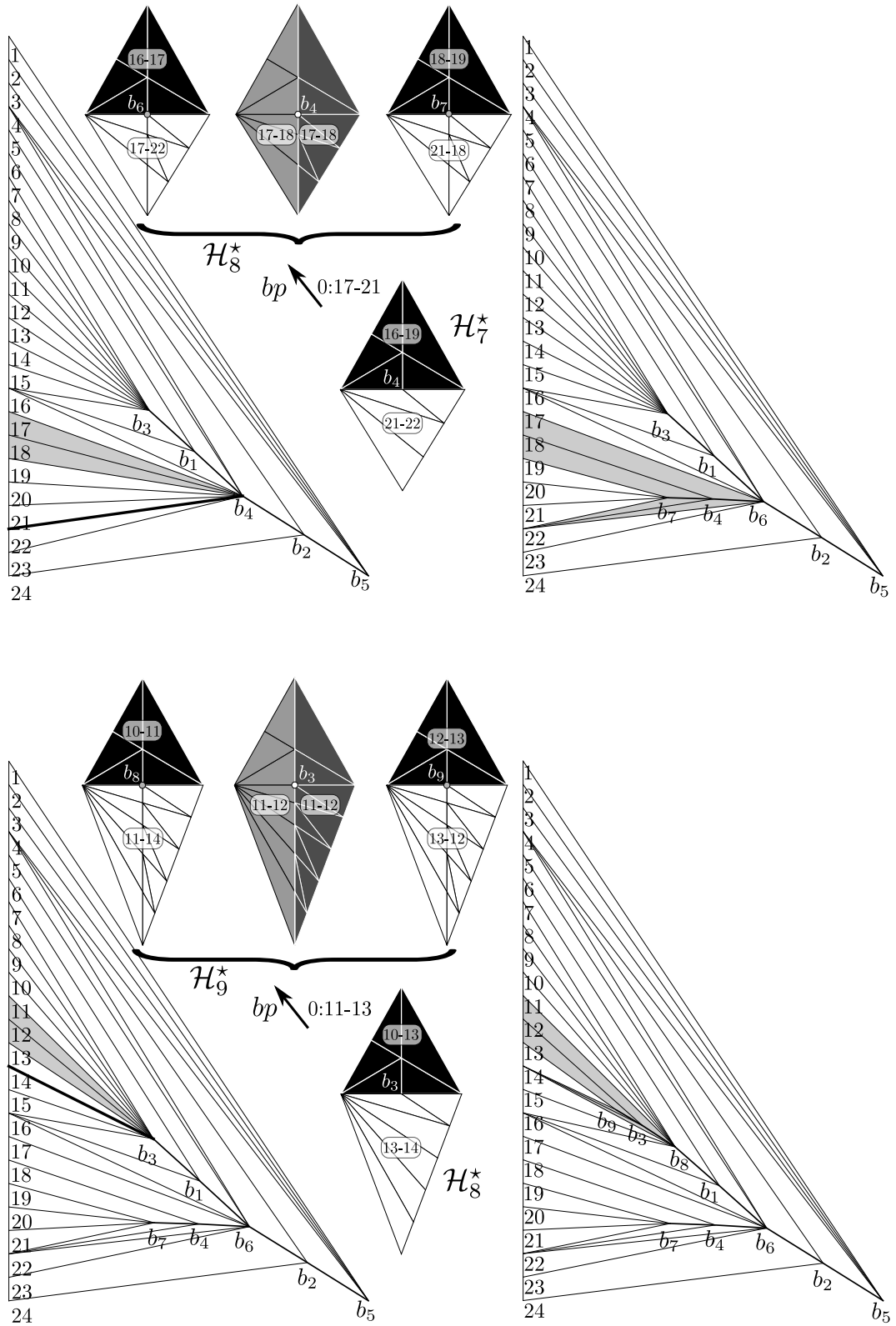


Figure 20: Right wings of complexes \mathcal{H}_7^* , \mathcal{H}_8^* and right wings of complexes \mathcal{H}_8^* , \mathcal{H}_9^* of the r_5^{24} example

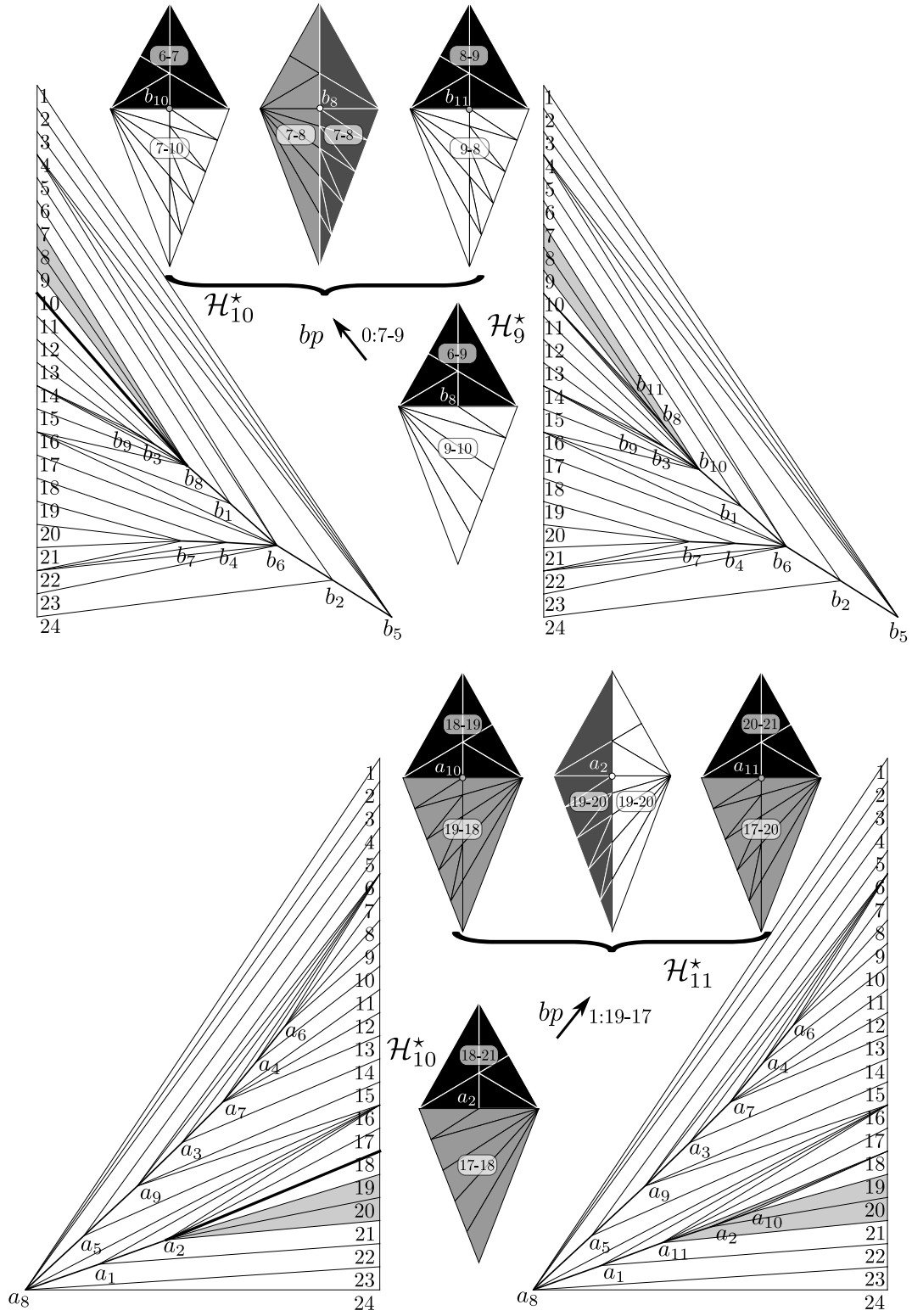


Figure 21: Right wings of complexes \mathcal{H}_9^* , \mathcal{H}_{10}^* and left wings of complexes \mathcal{H}_{10}^* , \mathcal{H}_{11}^* of the r_5^{24} example

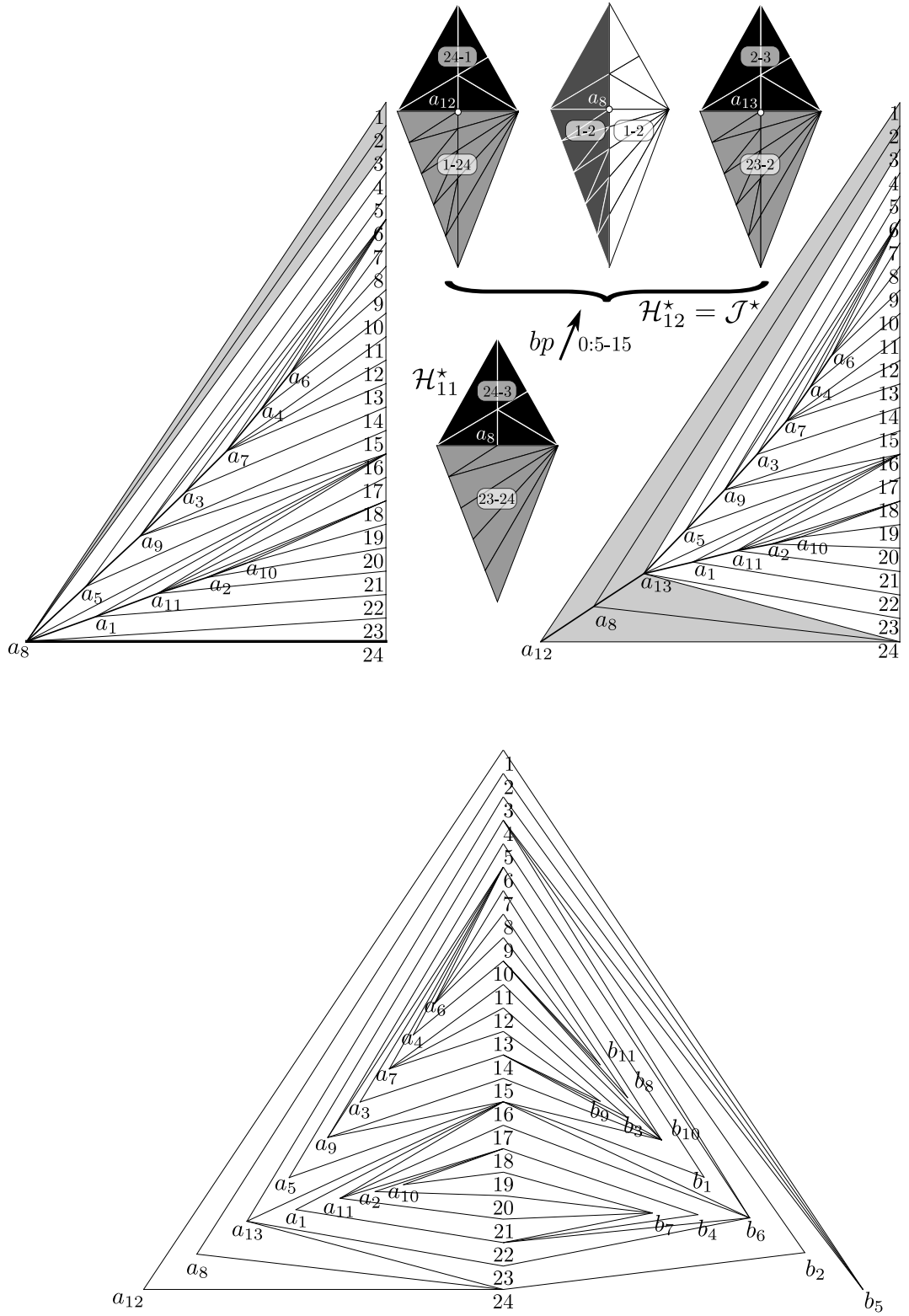


Figure 22: Left wings of complexes \mathcal{H}_{11}^* , \mathcal{H}_{12}^* and nervure-free wings of the final complex \mathcal{H}_{12}^* of the r_5^{24} example

Sóstenes L. Lins
Centro de Informática, UFPE
Recife-PE
Brazil
sostenes@cin.ufpe.br

Ricardo N. Machado
Núcleo de Formação de Docentes, UFPE
Caruaru-PE
Brazil
ricardonmachado@gmail.com